OXFORD

Human Molecular Genetics, 2018, Vol. 27, No. 3 451–462

doi: 10.1093/hmg/ddx414
Advance Access Publication Date: 28 November 2017
Original Article

ORIGINAL ARTICLE

Mouse models of two missense mutations in actin-binding domain 1 of dystrophin associated with Duchenne or Becker muscular dystrophy

Jackie L. McCourt[1,†], Dana M. Talsness[1,†], Angus Lindsay[2], Robert W. Arpke[3], Paul D. Chatterton[1], D'anna M. Nelson[1], Christopher M. Chamberlain[1], John T. Olthoff[1], Joseph J. Belanto[1], Preston M. McCourt[1], Michael Kyba[3], Dawn A. Lowe[2] and James M. Ervasti[1,*]

[1]Department of Biochemistry, Molecular Biology and Biophysics, [2]Department of Physical Medicine and Rehabilitation and [3]Department of Pediatrics University of Minnesota – Twin Cities, Minneapolis, MN 55455, USA

*To whom correspondence should be addressed. Tel: +1 6126266517; Fax: +1 6126252163; Email: jervasti@umn.edu

Abstract

Missense mutations in the dystrophin protein can cause Duchenne muscular dystrophy (DMD) or Becker muscular dystrophy (BMD) through an undefined pathomechanism. *In vitro* studies suggest that missense mutations in the N-terminal actin-binding domain (ABD1) cause protein instability, and cultured myoblast studies reveal decreased expression levels that can be restored to wild-type with proteasome inhibitors. To further elucidate the pathophysiology of missense dystrophin *in vivo*, we generated two transgenic *mdx* mouse lines expressing L54R or L172H mutant dystrophin, which correspond to missense mutations identified in human patients with DMD or BMD, respectively. Our biochemical, histologic and physiologic analysis of the L54R and L172H mice show decreased levels of dystrophin which are proportional to the phenotypic severity. Proteasome inhibitors were ineffective in both the L54R and L172H mice, yet mice homozygous for the L172H transgene were able to express even higher levels of dystrophin which caused further improvements in muscle histology and physiology. Given that missense dystrophin is likely being degraded by the proteasome but whole body proteasome inhibition was not possible, we screened for ubiquitin-conjugating enzymes involved in targeting dystrophin to the proteasome. A myoblast cell line expressing L54R mutant dystrophin was screened with an siRNA library targeting E1, E2 and E3 ligases which identified Amn1, FBXO33, Zfand5 and Trim75. Our study establishes new mouse models of dystrophinopathy and identifies candidate E3 ligases that may specifically regulate dystrophin protein turnover *in vivo*.

Introduction

The X-linked recessive disease Duchenne muscular dystrophy (DMD) is caused by mutations in the DMD gene that encodes the 427-kDa protein dystrophin (1). Dystrophin is predominantly expressed in muscle cells and is a critical component of the dystrophin–glycoprotein complex (DGC) that functions to stabilize the muscle cell membrane during muscle contraction (2,3). Disease-causing mutations in the DMD gene vary, with 68.5% of patients harboring large deletions (>1 exon), 11% with

[†]The authors wish it to be known that, in their opinion, the first two authors should be regarded as joint First Authors.

Received: August 27, 2017. **Revised:** October 12, 2017. **Accepted:** November 17, 2017

duplications (>1 exon), 10.2% with nonsense mutations, 6% with smaller deletions or insertions (<1 exon), 3% with splice-site mutations, 0.3% with mid-intronic mutations and 0.4% with missense mutations (4). Typically, mutations that result in the absence of dystrophin protein (i.e. through nonsense mutations or out-of-frame deletions) cause the severe phenotype of DMD (OMIM 310200) whereas mutations that result in a partially functional dystrophin protein cause a milder form known as Becker muscular dystrophy (BMD) (OMIM 300376) (5). Although very rare, disease-causing missense mutations provide unique opportunities to better understand the mechanism of dystrophinopathies. For example, a patient with an L54R mutation in the first calponin homology module (CH1) of actin-binding domain (ABD1) presented with DMD (6), while a patient with milder BMD was found to harbor an L172H mutation in the analogous location within CH2 of ABD1 (7).

In contrast to predictions that most disease-causing mutations in ABD1 would disrupt actin-binding activity (8), *in vitro* binding studies showed that several ABD1 missense mutations including L54R and L172H had minimal effect on the actin-binding affinity of full-length dystrophin (9). Additional experiments showed that ABD1 missense mutations compromised the thermal stability of dystrophin and increased the propensity for aggregation *in vitro* (9,10). Myoblast cell culture models expressing L54R or L172H dystrophins revealed a decrease in the steady state protein levels compared with wild-type dystrophin when normalized to the level of mRNA expression. L54R protein levels were lower than L172H levels, such that protein abundance was inversely proportional to the *in vitro* stability and the disease severity reported for the respective patients (11). Importantly, there was no mutant dystrophin protein observed in insoluble fractions from the cells and inhibition of autophagy had no effect on dystrophin protein abundance, both of which indicate there was no aggregation of the protein occurring in the cell culture model. Treatment of the L54R and L172H myoblast lines with proteasome inhibitors, however, did restore missense-mutant dystrophin expression to wild-type levels (11). These results suggested that missense mutant dystrophin is misfolded and subsequently degraded via the ubiquitin proteasome system, and that the percentage of protein targeted for degradation is directly related to how severely the mutation affects protein folding and stability. We hypothesized that misfolded dystrophins are being specifically targeted to the proteasome and that if degradation is inhibited the protein may still be functional. However, there is no method for assessing dystrophin functionality in cultured myoblasts.

Here we report the characterization of two new transgenic *mdx* mouse models expressing L54R (DMD) or L172H (BMD) mutant, full-length dystrophin. Phenotypic analysis of hemizygous L54R and L172H mice, as well as a homozygous L172H line, revealed a correlation between the levels of mutant dystrophin protein and improvement in some parameters of dystrophy. We have also identified four E3 ubiquitin ligases that impact missense dystrophin levels in cultured myoblasts and are candidates for modulation in the transgenic mouse models. The L54R and L172H mice will be useful tools in continuing to define the mechanism of mutant dystrophin turnover and molecular pathomechanisms of DMD and BMD.

Results

We generated transgenic mice expressing the L54R or L172H missense mutations in full-length dystrophin driven by the human skeletal actin (HSA) promoter and bred them onto the dystrophin-deficient *mdx* mouse line (labeled as mL54R and mL172H mice). Tibialis anterior, gastrocnemius and heart tissues were analyzed by RT-qPCR and western blot for dystrophin transcript and protein levels, respectively (Fig. 1). Both lines expressed the transgene in skeletal muscle, but not in the heart as expected based on the tissue specificity of the HSA promoter (12). The mL54R mice had dystrophin transcript levels not different from wild-type mice (Fig. 1A) but only 7–9% of wild-type protein levels (Fig. 1E). Transcript levels in mL172H mice were also not different from wild-type (Fig. 1B) but mutant protein levels were only 44% of wild-type (Fig. 1F). L54R and L172H protein levels were remarkably similar to the levels previously measured (11) in the respective C2C12 myoblast cell culture models (13% for L54R and 46% for L172H). The decrease in steady-state protein levels in the cell culture models was attributed to protein misfolding and subsequent degradation by the proteasome (11). To determine whether misfolded dystrophin in the new mouse models was stimulating a heat shock response or an unfolded protein response (UPR), several indicator proteins were analyzed by western blot (Supplementary Material, Fig. S1). We found that neither a heat shock response nor an UPR was elicited in the mL54R or mL172H mice.

To characterize the canonical signs of dystrophinopathy, 3-month-old mice were assessed for a number of cellular, histologic and physiologic parameters. The mL54R and mL172H mouse lines were analyzed for quantity and localization of several components of the DGC compared with wild-type and *mdx* mice (Fig. 2). The mutant dystrophin itself appeared to localize to the sarcolemma and no puncta or diffuse cytoplasmic staining were observed in the interior of the cells, indicating that although protein levels are decreased none of the mutant protein is aggregating (Fig. 2C). None of the missense dystrophin protein is detectably ubiquitinated (Supplementary Material, Fig. S2). Neither mL54R nor mL172H dystrophin restored any of the DGC components to wild-type expression levels (Fig. 2A and B), but DGC components did show proper sarcolemmal localization (Fig. 2C). Increased utrophin and decreased nNOS expression are often used as indicators of a dystrophic phenotype (13,14). Interestingly, utrophin expression in mL54R and mL172H lines was increased to the same degree as *mdx*, while nNOS expression was decreased but to a lesser extent than *mdx* in mL172H mice (Fig. 2A and B).

In addition to perturbations in assembly of the DGC, it has been demonstrated that dystrophin deficiency is associated with perturbations in subsarcolemmal microtubule lattice organization (15). Thus, we imaged and quantitatively assessed the microtubule lattice organization of extensor digitorum longus (EDL) muscle fibers in each mouse line (Fig. 3). Fibers from mL54R mice exhibited microtubule directionality significantly different from wild-type and resembling *mdx* fibers, whereas mL172H fibers restored microtubule organization from an *mdx* phenotype to not different from wild-type. The difference in microtubule lattice rescue between mL54R and mL172H mice may simply be owing to differences in protein abundance but may also reflect different effects of each mutation on dystrophin function.

Quadriceps muscle sections from the transgenic mice were stained with H&E and assessed for histologic signs of dystrophy (Fig. 4A). The mL54R line showed dystrophic features similar to *mdx*. The mL172H was also dystrophic, but possibly to a lesser degree. To quantify the histologic features, the centrally nucleated fibers (CNF) were counted as a percentage of total fibers (Fig. 4B). The data revealed that mL54R and mL172H lines had significantly increased CNFs over wild-type, but with lower

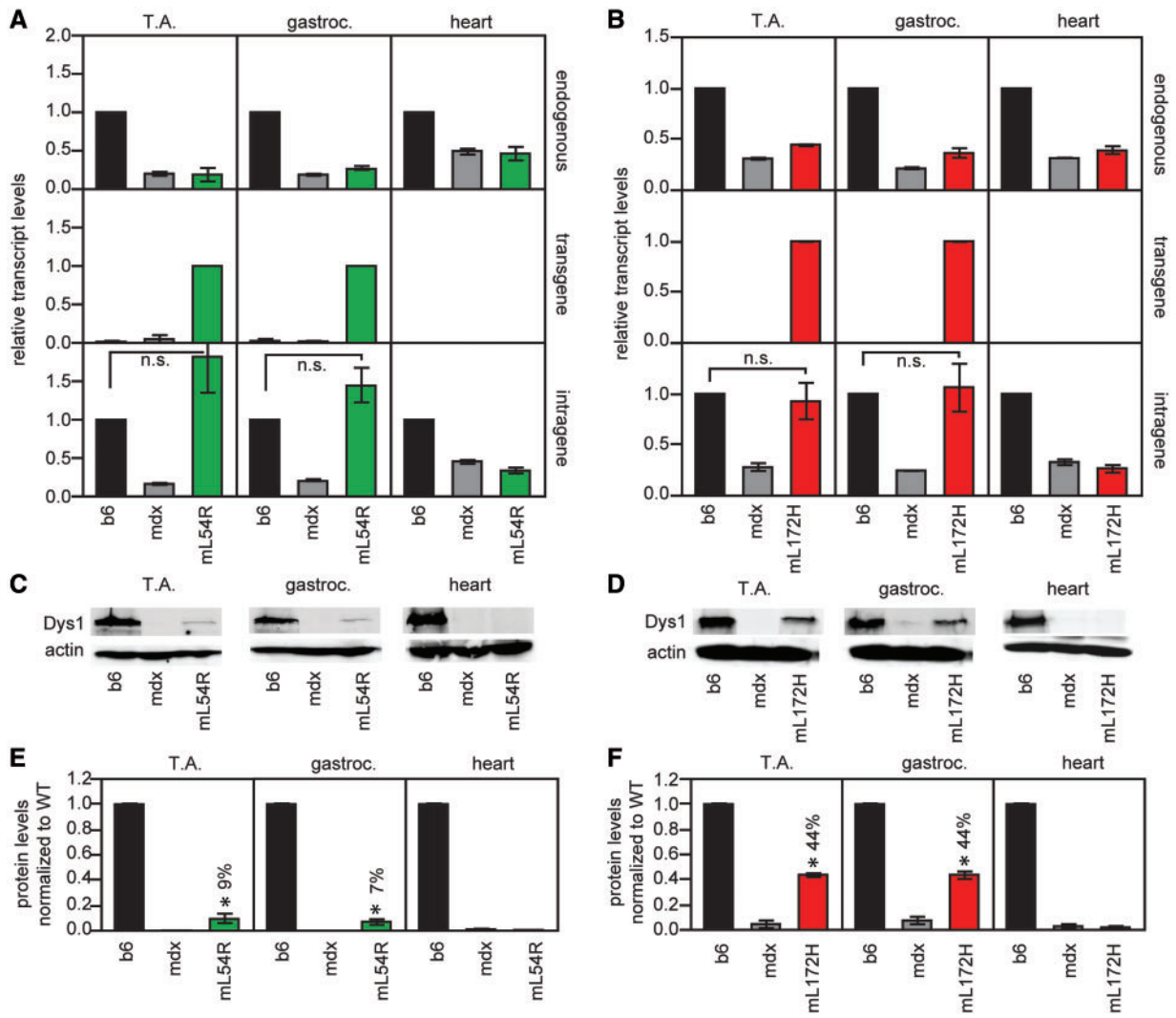

Figure 1. RNA and protein expression levels in transgenic mouse lines. (**A** and **B**) RT-qPCR analysis for mouse lines L54R and L172H, respectively. Top panel shows amplification within the 3'UTR of endogenous mouse dystrophin. Middle panel shows amplification within the 3'UTR of the transgenic dystrophin. Bottom panel shows amplification within the coding region of dystrophin, amplifying both endogenous and transgenic dystrophin. $n = 3$ separate animals for each line. ANOVA analysis of the intragene amplifications were $F < 0.05$ for both L54R and L172H lines. Post hoc analysis between b6 and transgenic were n.s. (not significant). (**C** and **D**) Representative western blot analyses of mouse lines L54R and L172H, respectively. (**E**) and (**F**) Quantification of western blots from $n = 3$ separate animals for each line. ANOVA analysis for both lines gave $F < 0.05$. Post hoc analysis $^*P < 0.05$ compared with b6.

average values than *mdx*. Indeed mL172H quadriceps had significantly lower CNFs than both *mdx* and mL54R. Across the four phenotypes, CNF values correlated inversely with dystrophin protein quantity (Fig. 4D). As an indicator of sarcolemmal integrity, creatine kinase (CK) activity was measured in the serum from each line of mice (Fig. 4C). Serum from *mdx* had significantly elevated activity compared with wild-type. Both mL54R and mL172H had intermediate levels of CK activity, being neither significantly different from wild-type nor *mdx*.

The transgenic mL54R and mL172H lines were assessed for several physiologic impairments associated with muscular dystrophy in the *mdx* mouse, including grip strength, whole body tension, activity after exercise and eccentric contraction-induced force loss (Fig. 5) (16–18). We found that for grip strength, whole body tension and activity after exercise (Fig. 5A–C) *mdx*, mL54R and mL172H all performed significantly worse than wild-type with no apparent rescue in the mL54R mouse or L172H compared with *mdx*. As a final assessment of physiologic performance, EDL muscles were analyzed *ex vivo* for force loss after eccentric contractions (Fig. 5D). Wild-type mice maintained the same level of force after five eccentric contractions, while *mdx*, mL54R and mL172H all dropped to ~20% of initial force by the fifth eccentric contraction. A summary of *ex vivo* parameters measured (Supplementary Material, Table S1) shows that all three of the dystrophic models were significantly different than wild-type for specific force, change in specific force after eccentric contractions, and percent force drop during eccentric contraction. Together, these data indicate that neither missense mutant line was different from *mdx*, suggesting that the L54R and L172H dystrophin proteins do not restore physiologic function at their given expression levels, while wild-type dystrophin at these same expression levels causes measureable phenotypic improvement (19,20).

Given that many of the cellular and histologic parameters measured, including nNOS expression (Fig. 2B), microtubule organization (Fig. 3), and %CNF (Fig. 4B) all showed dystrophic

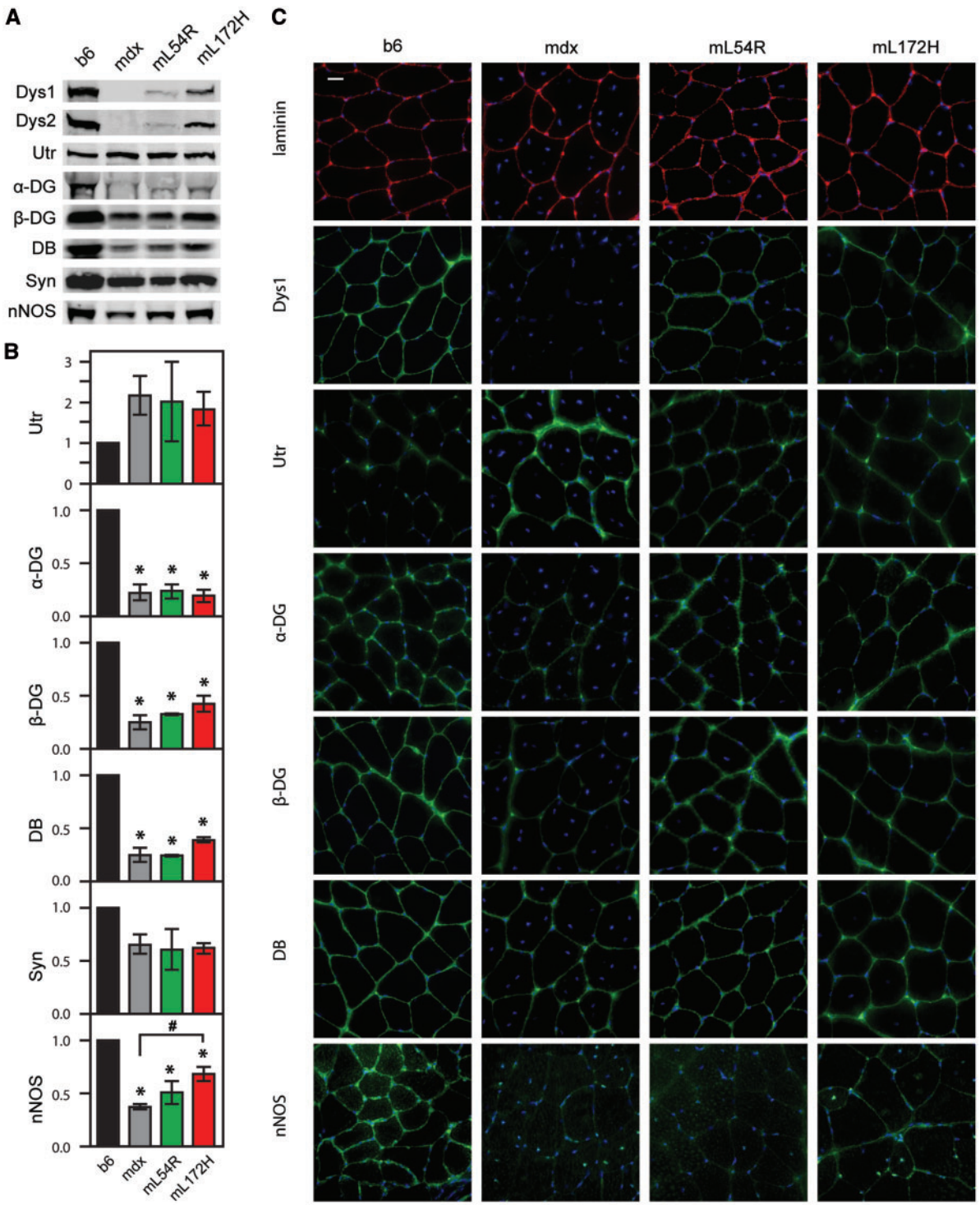

Figure 2. Expression levels and localization of components in the dystrophin–glycoprotein complex. Utr, utrophin; α-DG, alpha-dystroglycan; β-DG, beta-dystroglycan; DB, dystrobrevin; Syn, syntrophin; nNOS, neuronal nitric oxide synthase. (**A**) Representative western blot analyses for several components of the DGC in tibialis anterior muscle, including two different antibodies for dystrophin corroborating results found in Figure 1. (**B**) Quantification of western blots for $n = 3$ separate animals for each line. Values are all normalized to b6 values for each blot. ANOVA with significance of $F < 0.05$ were analyzed with post hoc statistics. $^{*}P < 0.05$ compared with b6. $^{\#}P < 0.05$ between *mdx* and L172H. (**C**) Immunofluorescent analysis of components of the DGC in quadriceps muscle. Scale bar = 20 μm.

phenotypes that correlated with disease severity, it was contradictory that none of the physiologic tests showed improvement over *mdx*. To test whether further increasing mutant dystrophin levels can improve the physiologic phenotypes of *mdx* mice, we generated and characterized mice homozygous for the L172H missense mutant dystrophin transgene (mhomL172H). By western blot, skeletal muscle from mhomL172H mice expressed significantly more dystrophin (~1.5×) than mL172H muscle (Fig. 6).

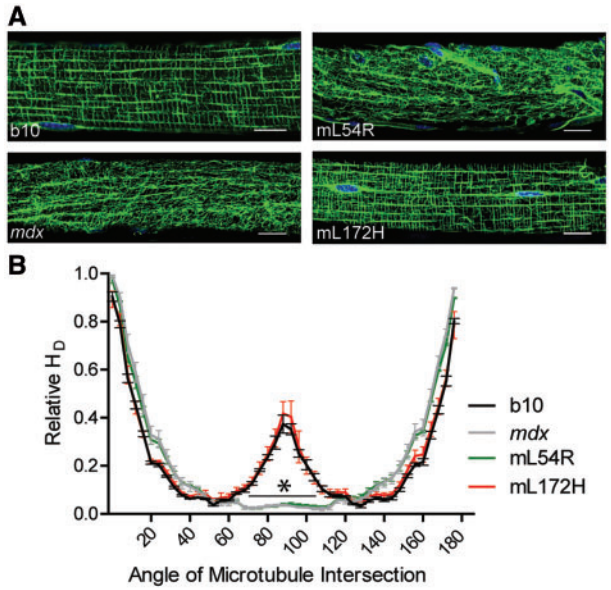

Figure 3. Microtubule lattice organization. (**A**) Images of microtubules (green) and nuclei (blue, DAPI) beneath the sarcolemma in b10, *mdx*, mL54R and mL172H mice. Images are representative of those obtained for $n \geq 10$ fibers from each of $n \geq 3$ mice per genotype. Bar, 20 μm. (**B**) Quantitative assessment of microtubule lattice organization as measured by transverse (90°) and longitudinal (0° and 180°) microtubules. Statistics were performed using two-way ANOVA with post hoc *t*-test analysis, $^*P < 0.001$ compared with b10.

Histologically, mhomL172H mice showed a further significant decrease in the number of CNF compared with mL172H mice (Fig. 7A and B). The mhomL172H animals demonstrated a modest but still significant protection from eccentric contraction-induced force loss compared with *mdx* and hemizygous mL172H littermates (Fig. 7C). Significant protection was measured for both lines when the eccentric contraction protocol was reduced from a 10% length change (Fig. 7C) to 5% during the eccentric contractions (Fig. 7D). Furthermore, mhomL172H mice showed significant improvements in specific force and eccentric contraction-induced force drop compared with *mdx*, which were not improved for mL172H mice (Supplementary Material, Table S2). Overall our results in homozygous L172H mice demonstrate phenotypic improvement with sufficiently high levels of missense mutant dystrophin.

We have previously demonstrated that L54R and L172H dystrophin levels increase in cultured C2C12 myoblasts following proteasome inhibitor treatment (11), and proteasome inhibitors have shown short-term efficacy in *mdx* mice (21–24). Therefore, we attempted to pharmacologically increase missense dystrophins by treating the mL54R and mL172H mice with several different proteasome inhibitors at various concentrations and by multiple delivery methods according to previously published protocols (Supplementary Material, Table S3; 21–27). Surprisingly, none of the proteasome treatments caused a detectable increase in dystrophin protein levels (Supplementary Material, Table S3 and Fig. S3). The discrepancy we observe in proteasome inhibitor effectiveness between cultured myoblasts and our transgenic mouse lines could be explained by differences in *in vitro* concentrations of inhibitor compared with therapeutic doses used in the mice (28,29).

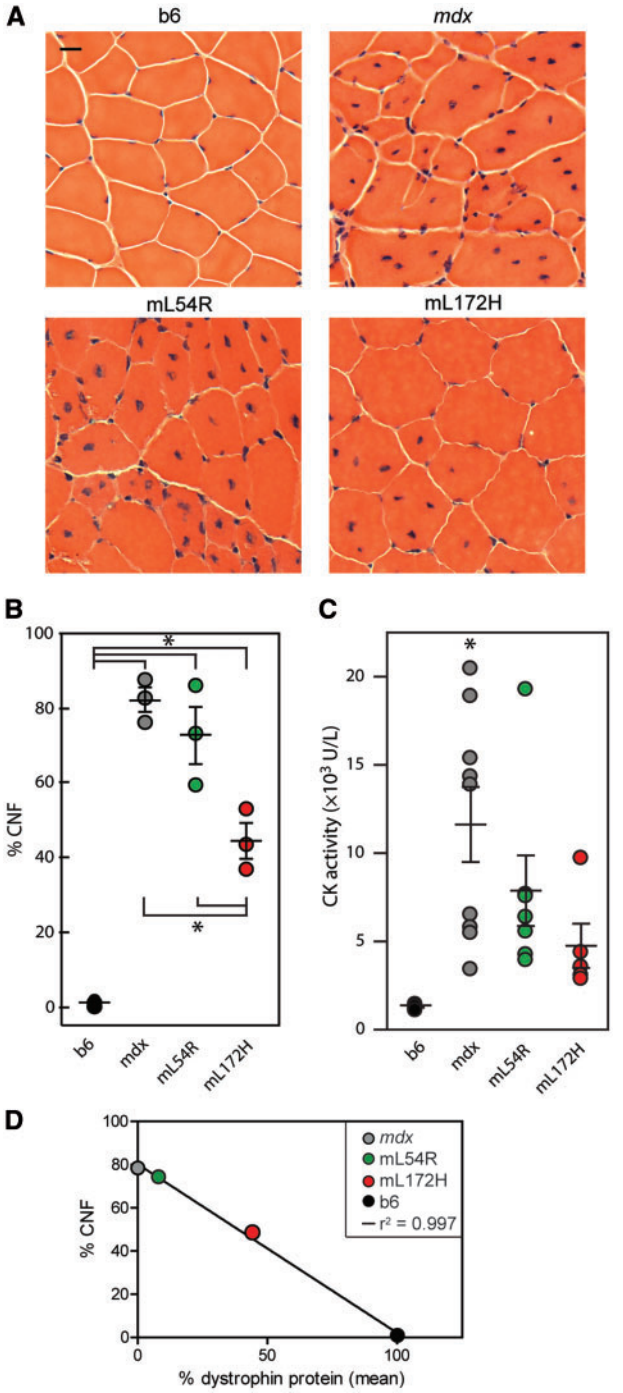

Figure 4. Fiber morphology and permeability. (**A**) Representative quadriceps muscle sections stained with H&E and imaged at × 20 magnification. Scale bar = 20 μm. (**B**) Quantification of centrally nucleated fibers (CNF) as a percentage of the total fibers. A minimum of 250 fibers were counted for each mouse. $n = 5$ for b6 and *mdx*, $n = 6$ for mL54R and mL172H. ANOVA analysis was significant at $F < 0.0001$. Post hoc analysis gave $^*P < 0.001$ for b6 mice versus all disease models, and for mL172H versus *mdx* and mL54R. (**C**) Serum creatine kinase (CK) activity from cheek bleeds of individual mice. $n = 5$ for b6, $n = 9$ for *mdx*, $n = 7$ for mL54R, $n = 9$ for mL172H. ANOVA analysis was significant at $F < 0.01$. Post hoc analysis gave $^*P < 0.01$ for b6 versus *mdx*. Both transgenic lines were not statistically different from b6 mice. (**D**) Analysis of % dystrophin protein versus %CNF. Line of best fit indicates a negative correlation.

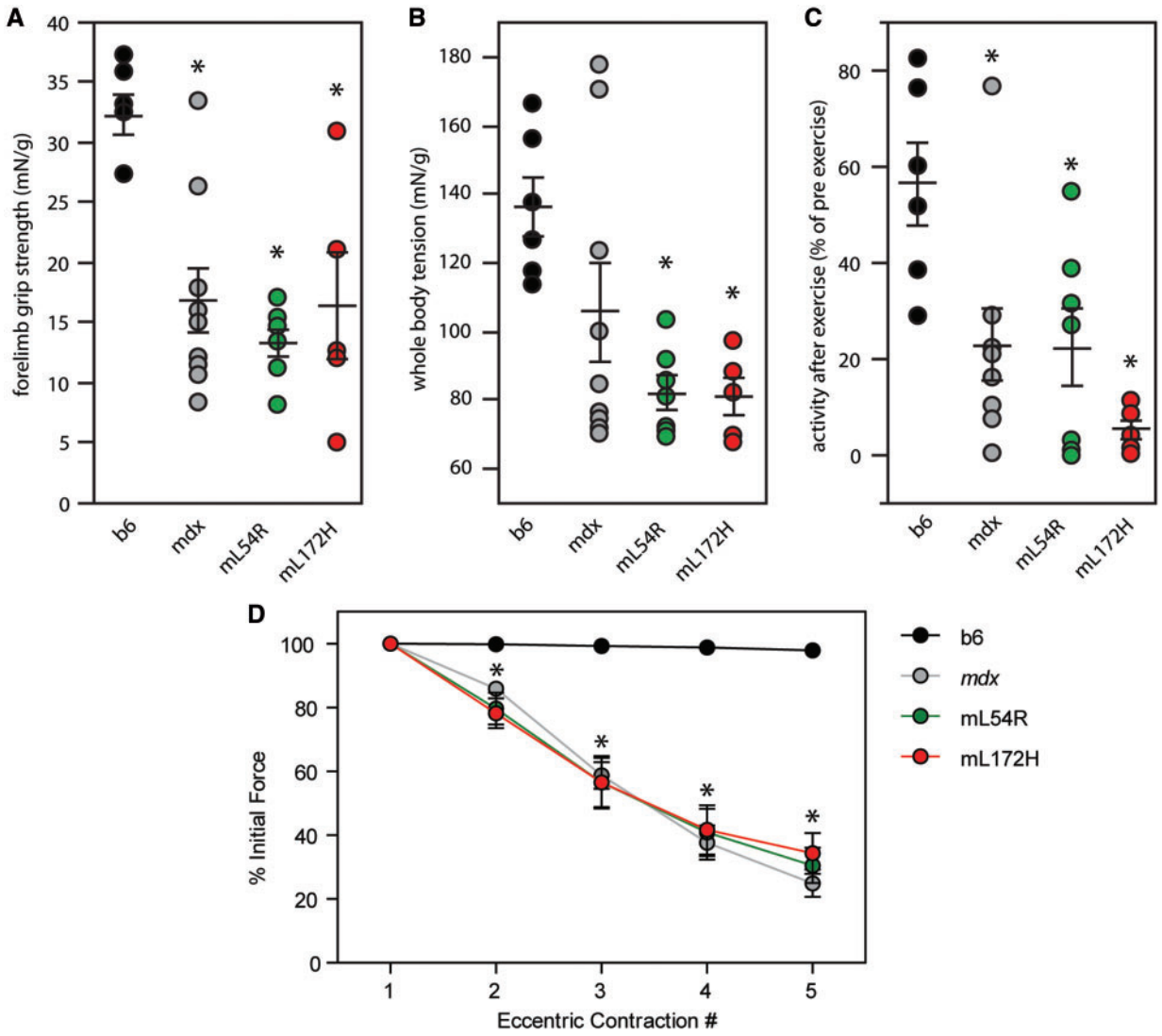

Figure 5. Physiology of transgenic mouse models. $n = 6$ for b6, $n = 9$ for *mdx*, $n = 7$ for mL54R, $n = 5$ for mL172H. (**A**) Forelimb grip strength analysis. Individual points are an average of five trials for each mouse. ANOVA was significant at $F < 0.001$. Post hoc analysis gave $^*P < 0.005$ compared with b6. (**B**) Whole body tension analysis. Individual points are an average of five trials for each mouse. ANOVA was significant at $F < 0.01$. Post hoc analysis gave $^*P < 0.05$ compared with b6. (**C**) Activity after exercise analysis. ANOVA was significant at $F < 0.005$. Post hoc analysis gave $^*P < 0.05$ compared with b6. (**D**) *Ex vivo* EDL force measurement during eccentric contraction. $n = 4$ for b6, $n = 5$ for *mdx*, $n = 6$ for mL54R, $n = 5$ for mL172H. Data for b6 mice taken from (15). For ECC 2–5, all three dystrophic models were significantly different than b6 mice.

Higher doses of proteasome inhibitor would likely lead to the toxicity that motivated cancer biologists to identify specific E3 ubiquitin ligases that target cancer-related proteins to the proteasome (30). Given our inability to sufficiently inhibit the proteasome and curiosity to begin to define the mechanism of dystrophin degradation, we performed an siRNA screen to identify the specific ubiquitin-conjugating enzymes that target missense mutant dystrophin to the proteasome. We used a myoblast cell line expressing GFP-tagged L54R dystrophin (11) to screen a commercial library of 512 different E1, E2 and E3 ligases by flow cytometry. From the 512 targets, 6 positive hits (Fig. 8A) were identified as those with fluorescence values significantly above the background threshold, indicating an increased level of the mutant dystrophin protein (Fig. 8B). All of the targets identified (ASB5, Trim75, Amn1, FBXO33, Zfand5 and TRAF2) are confirmed or putative E3 ubiquitin ligases. The six candidates were tested for specific effects in the cell culture model to determine whether the siRNA generated a significant knock-down of the target transcript. RT-qPCR for each respective transcript revealed that four of the six candidates were significantly knocked-down (Supplementary Material, Fig. S4). The myoblast models have previously shown that missense dystrophins are targeted to the proteasome (11), and now we have identified four candidate E3 ligases, FBXO33, Amn1, Zfand5 and Trim75, involved in the degradation of dystrophin, either by direct ubiquitination or by indirect means.

Discussion

We have generated two novel transgenic mouse lines modeling different missense mutations in ABD1 associated with DMD (L54R) or BMD (L172H). The original reports of missense mutations L54R and L172H were more than a decade apart from each other and therefore could not be compared side by side (6,7).

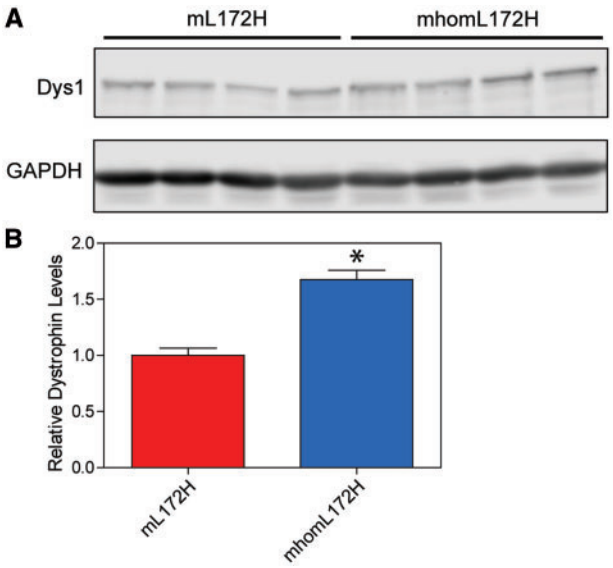

Figure 6. Dystrophin protein expression levels in transgenic homozygous L172H mice. (**A**) Dystrophin (Dys1) western blot of gastrocnemius muscle of hemizygous littermates (mL172H, $n=4$), and homozygous mice (mhomL172H, $n=4$) with GAPDH loading control. (**B**) Quantification of western blots. Unpaired *t*-test, $^{*}P<0.05$.

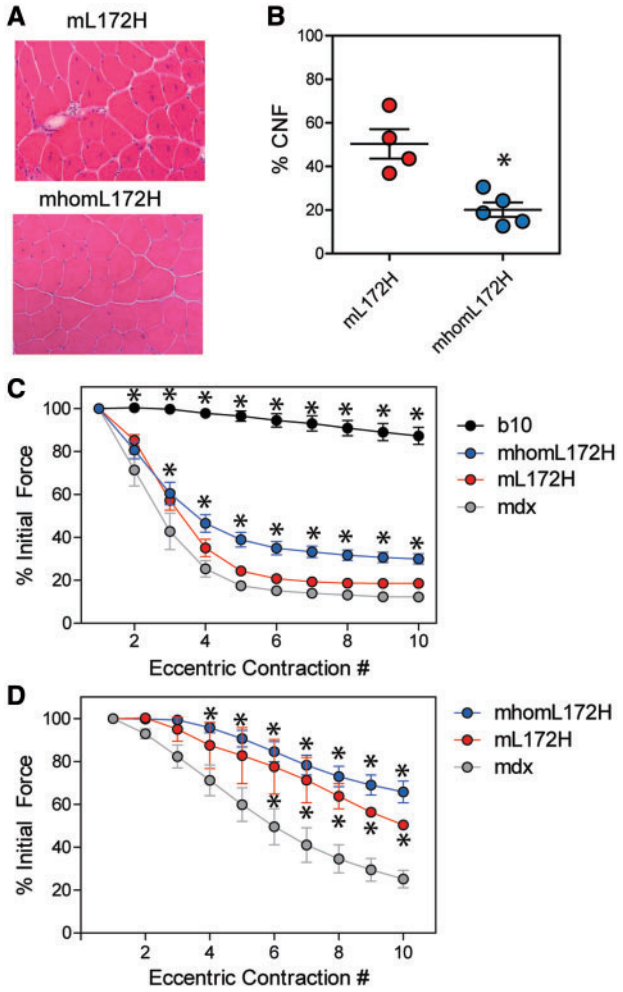

Figure 7. Histologic and physiologic analysis of transgenic homozygous L172H mice. (**A**) Representative quadriceps muscle sections from homozygous mice (mhomL172H) and hemizygous mice (mL172H) stained with H&E and imaged at × 20 magnification. Scale bar = 20 μm. (**B**) Quantification of centrally nucleated fibers (CNF) as a percentage of the total fibers. A minimum of 250 fibers were counted for each mouse ($n=3$). Unpaired *t*-test, $^{*}P<0.05$. *Ex vivo* EDL force measurement during eccentric contraction at 10% lengthening (**C**) or 5% lengthening (**D**). b10 $n=3$, *mdx* $n=3$, mL172H $n=6$ (10%) or $n=3$ (5%), mhomL172H $n=10$ (10%) or $n=4$ (5%); ANOVA, post hoc analysis gave $^{*}P<0.05$ compared with *mdx*.

While the pathophysiology of the patients was well reported (L54R with severe DMD phenotypes and L172H with mild BMD phenotypes), the molecular analysis was minimal, with each group estimating that their respective patient expressed dystrophin at 20% of normal control levels. Here we measured steady state dystrophin levels of 7–9% for L54R and 44% for L172H, which corroborate the level of each protein previously measured in the cell culture models, and is consistent with the degree of misfolding measured *in vitro* using differential scanning fluorimetry (11). The mL54R line presented with biochemical, histologic and physiologic phenotypes not different from the *mdx* mouse, whereas the mL172H line presented with a milder phenotype for several parameters tested. Therefore, it appears that the abundance of missense mutant dystrophin inversely correlates with disease severity in mice and we believe this is the major mechanism of disease.

Previous studies on the relationship between dystrophin protein expression and disease phenotype have also shown that disease severity inversely correlates with dystrophin protein levels (31,32). The first animal model with a missense mutation in dystrophin was reported in a line of pigs harboring a point mutation in Exon 41 resulting in full-length dystrophin with the amino acid change R1958W (33). Phenotypically, the R1958W pigs appear to most closely model mildly affected BMD patients and express dystrophin at 30% of wild-type levels. Transgenic *mdx* mice expressing only 20% of full-length dystrophin or a therapeutic mini-dystrophin demonstrated rescue of dystrophic phenotype (31,32). Therefore, our mL172H mouse line expressing 40% dystrophin levels should theoretically fully rescue the dystrophic phenotype, but instead only shows partial improvement in some parameters, suggesting that the L172H mutation disrupts dystrophin function in addition to protein stability. Other studies of dystrophin levels using non-transgenic mouse models with varying levels of dystrophin demonstrated that as little as 5% of wild-type dystrophin is sufficient to partially protect from some of the dystrophic phenotypes (20,34), suggesting that the L54R mutant expressed at 7–9% with no protection also has disrupted functionality.

To address the question of quality (dystrophin functionality) versus quantity (dystrophin levels), we generated homozygous transgenic mice. We hypothesized that a homozygous L54R mouse would not produce high enough dystrophin levels to see an improvement, thus we focused our efforts on generating and characterizing the L172H homozygous line. The homozygous mice showed >1.5-fold increase in dystrophin levels compared with hemizygous littermates, demonstrating that L172H mutant dystrophin levels are able to be manipulated. The homozygous L172H line showed significant improvements in central nucleation, specific force and eccentric contraction-induced force drop compared with hemizygous mice, indicating that higher levels of missense dystrophin are able to partially compensate for impaired functionality.

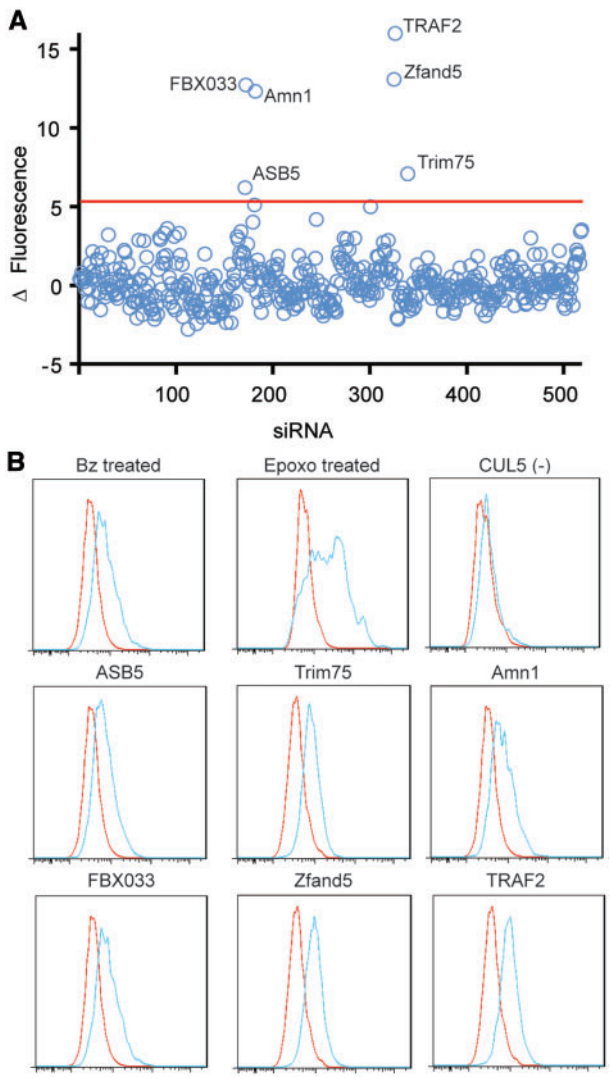

Figure 8. Flow cytometry results from siRNA screen of ubiquitin-conjugating enzymes. (**A**) Scatter plot of Δ Fluorescence for 512 targets in the siRNA library. The threshold (red line) was calculated using three standard deviations with six targets above the threshold. (**B**) Flow cytometry histogram plots generated from untreated cells (red plots), 1 μM bortezomib (Bz)-treated cells and 1 μM epoxomicin (epoxo) as proteasome inhibitor positive controls, a representative negative hit below the threshold (CUL5), and the six positive hits above the threshold.

In an attempt to pharmacologically increase mutant dystrophin protein, we treated mice with various proteasome inhibitors. In all cases, there was no evidence of increased dystrophin protein upon treatment, an observation that is in contrast to our previous work in cultured myoblasts that revealed a dose-dependent increase in missense dystrophin protein upon proteasome inhibitor treatment. At the therapeutic dose used *in vivo*, it is possible that only one type of proteasome active site, the chymotrypsin-like active site, is being targeted by the proteasome inhibitors thus leaving the caspase-like and trypsin-like sites functional to degrade missense dystrophins (35). At higher concentrations, as in the cultured myoblasts, the proteasome inhibitors are able to inhibit all three sites, and thus inhibit degradation of missense dystrophins, but would presumably be at toxic levels *in vivo* (11,28). Additionally, a study on the rates of protein degradation following proteasome inhibitor treatment showed that inhibition of the chymotrypsin-like site of the proteasome decreased protein degradation to a limited extent (<50%) and varied depending on the protein substrate being measured (35). It is also possible that the proteasome inhibitors are not targeting the muscle at sufficient concentrations to inhibit the proteasome or that only a small percentage of the proteasomes in muscle are being inhibited. Although proteasome inhibitors have demonstrated short-term efficacy in *mdx* mice (21,22,24), it would not be therapeutically practical to treat chronically ill patients with broad-spectrum proteasome inhibitors over the course of their lifetime. Thus, more recent approaches have focused on inhibitors of the ubiquitin-conjugating enzymes more specific to a given disease target (30).

Using a similar approach, we performed an siRNA screen that identified four E3 uibiquitin ligases that may be involved in targeting missense dystrophins to the proteasome. Zfand5, also known as Znf216, is a zinc-finger and AN1-like domain containing protein that has been shown to interact with IKKgamma (36) and, more notably, has been implicated in muscle atrophy (37). FBXO33 is a component of the SCF (Skp1/Cul1/F-box) E3 ubiquitin ligase (38), was identified as a seizure response gene (39) and as a target of the DUX4 transcription factor that is activated in facioscapulohumeral muscular dystrophy (40). Amn1 has been implicated in cell cycle regulation and a putative interactor with the E3 ligase APC (anaphase-promoting complex) (41). Trim75 is a tripartite motif containing protein identified as a female fertility factor (42) and, although other members of the Trim family of proteins such as Trim32 and Trim63 (also known as MURF1) have been studied in muscle pathologies (43,44), Trim75 function has not, to our knowledge, been studied in muscle. With the exception of FBXO33, the E3 ligases we identified have not been previously associated with muscular dystrophy and none of them have been reported to bind to or ubiquitinate dystrophin.

In contrast to cell stress conditions such as hypoxia or muscle atrophy where E3 ubiquitin ligases are upregulated (43,45), we see no evidence that our candidate dystrophin E3 ligases are upregulated in response to missense dystrophin proteins in our mouse models (Supplementary Material, Fig. S5). Furthermore, we do not observe an increase in heat shock pathway proteins or UPR proteins in the mice (Supplementary Material, Fig. S1), supporting the hypothesis that missense dystrophins are not stimulating a global misfolded protein response but are rather being regulated by specific E3 ligases already present in the cell for the purpose of protein homeostasis. In future studies, we aim to knockdown our candidate E3 ligases in transgenic missense dystrophin mice and generate knockout mice for cross breeding in order to evaluate the effect on missense dystrophin expression.

In summary, this work establishes two new transgenic *mdx* mouse lines modeling missense mutant dystrophins from actual patient mutations. The proposed primary mechanism of disease in these models is through degradation of misfolded missense dystrophin proteins via the ubiquitin-proteasome pathway. The implications of this work are not limited to missense mutants only but may also apply to other potentially misfolded dystrophin proteins, such as internally deleted dystrophins (46,47) found in BMD patients, those miniaturized dystrophins under investigation as therapeutic constructs for gene therapy, or in exon skipping therapies.

Materials and Methods

Cloning and mouse generation

Full-length mouse dystrophin cDNA (with missense mutations L54R and L172H) was subcloned into the Gateway system Entry vector (Life Technologies). The cDNA was then recombined into a vector containing the human skeletal alpha-actin (HSA) promoter and Vp1 intron that had been adapted to the Gateway system. The expression cassette was cut out of the vector with restriction enzymes and sent to the University of Cincinnati Transgenic Mouse Core (L54R) or The Scripps Research Institute Mouse Genetics Core (L172H) for pronuclear injection into fertilized eggs of C57BL/6J mice. Injected eggs were transplanted into pseudopregnant mice. Progeny were screened for the transgene by genomic PCR. Transgenic mice were crossed onto the *mdx* background (mL54R and mL172H), and transgenic male progeny were analyzed. Homozygous mice were generated by breeding transgene positive *mdx* males with transgene positive females. Progeny were then analyzed for homozygosity by genomic quantitative PCR using HSA transgene promoter specific primers as detailed below. All analyses were performed on mice 10–14 weeks of age and compared with C57BL/6J (b6) or C57BL/10J (b10) wild-type mice as noted.

RT-qPCR

Tissue was pulverized with mortar and pestle in liquid nitrogen. RNA was isolated with the Aurum Total RNA Fatty and Fibrous Tissue (BioRad 732-6870) or Aurum Total RNA kit (BioRad 732-6820) for C2C12 cells. Total RNA was reverse transcribed into cDNA (1 μg total for a concentration of 50 ng/μl) using the iScript™ Advanced cDNA Synthesis Kit (BioRad 170-8843). cDNA was then diluted to a concentration of 10 ng/μl to be used for amplification using SsoAdvanced™ Universal SYBR® Green Supermix (BioRad 172-5270). Primers for endogenous mouse dystrophin: Forward [TGGCAGATGATTTGGGCAGA] and Reverse [CCATGCGGGAATCAGGAGTT]. Primers for transgenic mouse dystrophin (for HSA transgene promoter): Forward [ACAATGTAGAAGGGTGGGCG] and Reverse [GCGTAGAATCGA GACGCGAGG]. Primers for intragenic mouse dystrophin: Forward [GCGCCAACACAAAGGACGCC] and Reverse [GCTTCAGCCTGGG GCTGCTC]. All measurements were normalized to reference transcript Hprt: Forward [CCCTGGTTAAGCAGTACAGCCCC] and Reverse [GGCCTGTATCCAACACTTCGAGAGG]. Primers for RT-qPCR of the siRNA positive hits are listed in the table below. Measurements were collected with the C1000 Touch Thermal Cycler (BioRad) and analyzed with the CFX Manager software (BioRad).

Western blot analysis

Tissue was pulverized with mortar and pestle in liquid nitrogen. Tissue was then lysed with 1% SDS solution with added protease inhibitors (100 nM Aprotinin, 10 mg/ml E-64, 100 μM Leupeptin, 1 mM PMSF, 1 μg/ml Pepstatin) proportional to mass of the tissue pellet. Protein concentration was measured by A_{280} absorbance. Equal concentrations of lysate were then separated by electrophoresis at 150 V for 1 h and transferred to PVDF membrane at 100 V/0.7 Amp for 1 h. Membranes were blocked in either (5% non-fat milk in PBS 0.1% Tween solution) or (5% bovine serum albumin in Tris-buffered saline 0.1% Tween solution) depending on the primary antibody for 1 h. Primary antibodies used were anti-Dys1 (Leica) at 1:100, anti-Dys2 (Leica) at 1:100, anti-utrophin (Santa Cruz 8A4) at 1:100, anti-α-dystroglycan (Millipore 05-593) at 1:1000, anti-β-dystroglycan (vector labs VP-B205) at 1:100, anti-dystrobrevin (BD labs 610766) at 1:1000, anti-syntrophin (Abcam 11425) at 1:1000, anti-pan actin C4 (Seven Hills Bioreagent LMAB-C4) at 1:5000, anti-desmin D93F5 (Cell Signaling 5332) at 1:1000, anti-Hsp40 C64B4 (Cell Signaling 4871) at 1:1000, anti-Hsp70 (Cell Signaling 4872) at 1:1000, anti-Hsp90 (Abcam 19021) at 1:1000, anti-Phosph-Hsp90α (Cell Signaling 3488) at 1:1000, anti-Phospho-Hsp27 (Cell Signaling 9709) at 1:1000, anti-Fbxo33 at 1:500 (Abcam ab90046), anti-Zfand5 at 1:500 (Abcam ab86560), anti-Trim75 at 1:500 (Aviva Systems Biology OAAB13204) anti-Amn1 at 1:500 (Boster Bio A15649), anti-PDI at 1:1000 (Cell Signaling C81H6), anti-IRE1α at 1:1000 (Cell Signaling 14C10) and anti-ubiquitin P4D1 at 1:1000 (Cell Signaling 3936). Blots were then incubated in secondary antibodies anti-mouse or anti-rabbit IgG Dylight® 800 (Cell Signaling) at 1:10 000 in blocking buffer. Secondary antibody signal was visualized on Licor's Odyssey® Infrared Imaging System and band density calculated with Odyssey Software v2.1. Pan actin C4 or REVERT™ total protein stain (Licor, according to the manufacturer's protocol) were used as loading controls.

Immunofluorescent analysis

Quadriceps and gastrocnemius muscles were dissected, frozen in melting isopentane, and embedded in optimum cutting temperature compound submerged in liquid nitrogen. Transverse sections of 10 μm were cut on a Leica CM3050 cryostat, air dried, and then fixed in 4% paraformaldehyde for 10 min. Sections were washed with PBS (150 mM NaCl, 8 mM NaH_2PO_4, 42 mM Na_2HPO_4) before being blocked with 5% goat serum/0.1% Triton X-100 for 30 min. A secondary block in Rodent Block M (Biocare Medical) was also performed for 30 min. The sections were then incubated with primary antibodies overnight at 4 °C. Primary antibody dilutions were: NCL-Dys1 (1:20) (Leica), NCL-Dys2 (1:20) (Leica), Rb2 (1:20), Utrophin (1:50) (Santa Cruz), α-Dystroglycan (1:50) (Millipore), β-Dystroglycan

Target	Forward primer	Reverse primer
ASB5	AAGCTGGGGCTAATGCAAAC	CAGGACTCCAGTTGGGCTTT
Amn1	GTCAGCTCCTGGAACTATGTCT	GTTATCCGACCCCGAATGCT
FBXO33	TTGGCAATTCATGGTTACACCG	GCCCAGTGATACCTGCTCAA
Zfand5	GTCACTCAGCCCAGTCCATC	GCAGTCAAACCCTGTAAGGC
TRAF2	GCTACTGCTCCTTCTGCCTG	TGGAAAGGCCGAACTACTCTC
Trim75	TCTTGGTAAGTCAACCGGGC	GGGTTTGGGCTGGTGATGTA

(1:50) (Vector Labs), Dystrobrevin (BD Biosciences), nNOS (1:50) (Invitrogen) and Laminin (1:1000) (Sigma). Sections were then washed with PBS and incubated with Alexa Fluor 488- or Alexa Fluor 568-conjugated secondary antibodies (1:500 dilutions) for 30 min at 37°C. Sections were washed with PBS and coverslips were applied with a drop of Prolong Gold antifade reagent with DAPI (Molecular Probes). Images were collected on a Deltavision PersonalDV microscope equipped with a 20×/0.75 objective (Applied Precision) and viewed with GIMP (GNU Image Manipulation Program) software.

Muscle fiber imaging

EDL muscles were harvested from 3- to 4-month old perfusion-fixed mice and immunostained for α-tubulin (DM1A). Perfusion media (50 mM Pipes, 5 mM EGTA, 2 mM $MgSO_4$, 10% (vol/vol) DMSO and 0.1% Triton X-100, pH 6.8) contained 4% (wt/vol) paraformaldehyde. Muscles were further post-fixed in 4% (wt/vol) paraformaldehyde in PBS (PBS: 8 mM NaH_2PO_4, 42 mM Na_2HPO_4 and 150 mM NaCl, pH 7.5) for 24 h while rotating. Single muscle fibers or bundles of two or three muscle fibers were mechanically teased apart and incubated with anti-α-tubulin antibody overnight with rotation. Goat anti-mouse secondary antibody coupled to Alexa Fluor 568 was used for visualization. Fibers were mounted on slides using SlowFade Gold antifade reagent with DAPI (Invitrogen) to visualize nuclei. Fibers were imaged on the Olympus FluoView FV1000 with the 60× oil immersion objective using the accompanying software. ImageJ sum slices projection was used to combine Z-stacks of two to three sarcolemmal images. Brightness and contrast were adjusted using ImageJ. Images are representative of $n \geq 3$ mice per genotype and $n \geq 10$ fibers per mouse.

Quantitative microtubule lattice analysis

Using a previously developed directionality analysis program (TeDT; (48)), microtubule lattice directionality was calculated for all mouse lines. A two-way ANOVA was used to assess the effect of microtubule intersection angle across groups. Bonferroni post hoc measures were used to determine the extent of differences between groups. Significance was set at $P < 0.05$.

Histology and CNF count

Cryosections were cut from the same blocks prepared for immunofluorescence at 10 μm thickness. Sections were stained with hematoxylin and eosin–phloxine and imaged on Leica DM5500 microscope at 20× total magnification. A total of at least 250 fibers were imaged from each muscle of each mouse and then CNF counted as a percentage of the total.

Serum CK analysis

Serum samples of the mice were collected by cheek bleed. The samples were diluted 1:20 and then serum CK activity analyzed using CK DT slides (Ortho-Clinical Diagnostics) and a Kodak Ektachem DT 60 Analyzer. CK activity is reported as U/L.

Forelimb grip strength

Mice were gripped at the base of their tail and positioned to grab the DFE series digital force gauge (Chatillon) with grip bar attachment. Once the mouse was gripping the bar with both hands, the mouse was slowly with consistent force pulled perpendicularly away from the grip bar. Five trials were run per mouse and the average force was calculated.

Whole body tension

Mice were placed between parallel barriers, allowing only for forward movement. A slipknot suture was used to attach the base of the mouse tail to a fixed range force transducer (BioPac Systems). The tail of the mouse was then lightly pinched and the subsequent force evoked was measured. Five minute traces were collected and the top five peaks were averaged for each mouse and then normalized to body weight. Protocol adapted from (49).

Activity after exercise

Mice were acclimatized to the treadmill for 3 consecutive days, for 5 min at 0 m/min followed by 5 min at 9 m/min at 0° decline. On the fourth day, baseline pre-exercise activity was assessed for 30 min using laser-sensor activity cages (AccuScan Instruments, Inc.). Mice were then acclimatized to the treadmill for 5 min at 0 m/min at 15° decline. Without the use of electrical shock, mice were then encouraged to walk on the treadmill for 5 min at 5 m/min followed by 10 min at 15 m/min. After exercise, activity was measured for 30 min. A total number of vertical episodes were counted and post-exercise activity reported as a percentage of the pre-exercise activity.

Eccentric contraction analysis

Mice were anesthetized with sodium pentobarbital and EDL muscle dissected. Silk suture was used to attach the distal tendon to a static structure and the proximal tendon to a force transducer (Model 300B-LR, Aurora Scientific). The EDL was incubated in Kreb-Ringer bicarbonate buffer [120.5 mM NaCl, 4.8 mM KCl, 1.2 mM $MgSO_4$ 1.2 mM Na_2HPO_4, 20.4 mM $NaHCO_3$, 10 mM glucose, 10 mM pyruvate, 1.5 mM $CaCl_2$], oxygenated with 95% O_2/5% CO_2. Muscles were lengthened to an optimal tension and this set as the optimal length (L_0). Maximal isometric twitch and tetanic forces were measured. For eccentric contraction experiments with 10% length change, the EDL muscle was stimulated (200 ms at 175 Hz) while simultaneously lengthening from 95% to 105% of the L_0 at 0.5/s. For eccentric contraction experiments with 5% length change, the EDL muscle was stimulated the same but lengthening was from 97.5% to 102.5% of the L_0 at 0.25 L_0/s. Three minutes recovery was allowed between each eccentric contraction and maximum eccentric force was recorded for each contraction. Eccentric force was plotted as a percentage of the first eccentric contraction.

Drug treatment of mice

Transgenic male mice between 10 and 14 weeks of age were treated with bortezomib (Cell Signaling 2204S), oprozomib (ApexBio A1934), carfilzomib (Selleckchem S2853), MG132 (Thermo Fisher AP81515A) or gedunin (Santa Cruz Biotechnology sc-203967) according to the conditions outlined in Supplementary Material, Table S3.

siRNA screen

The L54R mutant dystrophin C2C12 cell line was grown according to (11). Cells were seeded to 600 000 and adhered for 4 h

before being treated with mouse ON-TARGETplus siRNA library for Ubiquitin Conjugating Enzymes Subsets 1, 2 and 3 (Dharmacon). Cells were treated with 40 nM siRNA pools according to the manufacturer's protocol or treated with 1 μM bortezomib as a positive control. After 48 h, cells were trypsinized and resuspended with 50 μl fluorescence-activated cell sorting (FACS) staining medium: phosphate-buffered saline (PBS) (Mediatech, Inc., Manassas, VA, USA) containing 2% fetal bovine serum (HyClone, Logan, UT, USA) supplemented with 1 μg/ml propidium iodide. Flow cytometry analysis was performed on a BD FACSAriaII (BD Biosciences, San Diego, CA, USA) and data were analyzed using FlowJo (FlowJo LLC, Ashland, OR, USA). The screen was performed over 4 days with negative controls (untreated cells) and positive controls (bortezomib or epoxomicin) measured for each day. Change in fluorescence (Δ Fluorescence) was calculated by subtracting the negative control for each day and normalized to the median fluorescence for each day. The threshold was calculated using 3 standard deviations. To validate the positive hits, L54R C2C12 cells were seeded at 1×10^6 and adhered for 18 h before treatment with 40 nM of siRNA for 24 h.

Statistics

Data are presented as mean ± standard error of the mean. To determine significance for all data with three or more groups, one-way ANOVA analysis was performed with $\alpha = 0.05$. Upon significance of the ANOVA, Tukey post hoc tests were performed with all pairs of data at $\alpha = 0.05$.

Supplementary Material

Supplementary Material is available at *HMG* online.

Conflict of Interest statement. None declared.

Funding

The study was supported by National Institute of Arthritis and Musculoskeletal and Skin Diseases grant RO1 AR042423 to J.M.E. and R01 AR055685 to M.K. J.L.M., J.J.B. and J.T.O. were supported by the National Institutes of Health Training Program in Muscle Research (AR007612). J.J.B. was also supported by a University of Minnesota Doctoral Dissertation Fellowship. J.T.O. and D.M.N. were each supported by fellowships from the National Institute on Aging Training Program for Functional Proteomics of Aging (T32 AG029796). D.M.T. was supported by an American Heart Association Predoctoral Fellowship (12PRE12040402). C.M.C. was supported by Muscular Dystrophy Association grant MDA349549.

References

1. Koenig, M., Monaco, A.P. and Kunkel, L.M. (1988) The complete sequence of dystrophin predicts a rod-shaped cytoskeletal protein. *Cell*, **53**, 219–228.
2. Ervasti, J.M. (2003) Costameres: the Achilles' heel of Herculean muscle. *J. Biol. Chem.*, **278**, 13591–13594.
3. Rybakova, I.N., Patel, J.R. and Ervasti, J.M. (2000) The dystrophin complex forms a mechanically strong link between the sarcolemma and costameric actin. *J. Cell Biol.*, **150**, 1209.
4. Bladen, C.L., Salgado, D., Monges, S., Foncuberta, M.E., Kekou, K., Kosma, K., Dawkins, H., Lamont, L., Roy, A.J., Chamova, T. *et al.* (2015) The TREAT-NMD DMD global database: analysis of more than 7, 000 Duchenne muscular dystrophy mutations. *Hum. Mutat.*, **36**, 395–402.
5. Koenig, M., Beggs, A., Moyer, M., Scherpf, S., Heindrich, K., Bettecken, T., Meng, G., Müller, C.R., Lindlöf, M. and Kaariainen, H. (1989) The molecular basis for Duchenne versus Becker muscular dystrophy: correlation of severity with type of deletion. *Am. J. Hum. Genet.*, **45**, 498–506.
6. Prior, T.W., Papp, A.C., Snyder, P.J., Burghes, A.H.M., Bartolo, C., Sedra, M.S., Western, L.M. and Mendell, J.R. (1993) A missense mutation in the dystrophin gene in a Duchenne muscular dystrophy patient. *Nat. Genet.*, **4**, 357–360.
7. Hamed, S., Sutherland-Smith, A., Gorospe, J., Kendrick-Jones, J. and Hoffman, E. (2005) DNA sequence analysis for structure/function and mutation studies in Becker muscular dystrophy. *Clin. Genet.*, **68**, 69–79.
8. Norwood, F.L., Sutherland-Smith, A.J., Keep, N.H. and Kendrick-Jones, J. (2000) The structure of the N-terminal actin-binding domain of human dystrophin and how mutations in this domain may cause Duchenne or Becker muscular dystrophy. *Structure*, **8**, 481–491.
9. Henderson, D.M., Lee, A. and Ervasti, J.M. (2010) Disease-causing missense mutations in actin binding domain 1 of dystrophin induce thermodynamic instability and protein aggregation. *Proc. Natl. Acad. Sci. USA.*, **107**, 9632–9637.
10. Singh, S.M., Kongari, N., Cabello-Villegas, J. and Mallela, K.M.G. (2010) Missense mutations in dystrophin that trigger muscular dystrophy decrease protein stability and lead to cross-beta aggregates. *Proc. Natl. Acad. Sci. U. S. A*, **107**, 15069–15074.
11. Talsness, D.M., Belanto, J.J. and Ervasti, J.M. (2015) Disease-proportional proteasomal degradation of missense dystrophins. *Proc. Natl. Acad. Sci. USA.*, **112**, 12414–12419.
12. Jaeger, M.A., Sonnemann, K.J., Fitzsimons, D.P., Prins, K.W. and Ervasti, J.M. (2009) Context-dependent functional substitution of alpha-skeletal actin by gamma-cytoplasmic actin. *FASEB J.*, **23**, 2205–2214.
13. Matsumura, K., Ervasti, J.M., Ohlendieck, K., Kahl, S.D. and Campbell, K.P. (1992) Association of dystrophin-related protein with dystrophin-associated proteins in mdx mouse muscle. *Nature*, **360**, 588–591.
14. Brenman, J.E., Chao, D.S., Xia, H., Aldape, K. and Bredt, D.S. (1995) Nitric oxide synthase complexed with dystrophin and absent from skeletal muscle sarcolemma in Duchenne muscular dystrophy. *Cell*, **82**, 743–752.
15. Belanto, J.J., Mader, T.L., Eckhoff, M.D., Strandjord, D.M., Banks, G.B., Gardner, M.K., Lowe, D.A. and Ervasti, J.M. (2014) Microtubule binding distinguishes dystrophin from utrophin. *Proc. Natl. Acad. Sci. USA.*, **111**, 5723–5728.
16. Petrof, B.J., Shrager, J.B., Stedman, H.H., Kelly, A.M. and Sweeney, H.L. (1993) Dystrophin protects the sarcolemma from stresses developed during muscle contraction. *Proc. Natl. Acad. Sci. USA.*, **90**, 3710–3714.
17. Connolly, A.M., Keeling, R.M., Mehta, S., Pestronk, A. and Sanes, J.R. (2001) Three mouse models of muscular dystrophy: the natural history of strength and fatigue in dystrophin-, dystrophin/utrophin-, and laminin alpha2-deficient mice. *Neuromuscul. Disord.*, **11**, 703–712.
18. Kobayashi, Y.M., Rader, E.P., Crawford, R.W., Iyengar, N.K., Thedens, D.R., Faulkner, J.A., Parikh, S.V., Weiss, R.M., Chamberlain, J.S., Moore, S.A. *et al.* (2008) Sarcolemma-localized nNOS is required to maintain activity after mild exercise. *Nature*, **456**, 511–515.

19. Phelps, S.F., Hauser, M.A., Cole, N.M., Rafael, J.A., Hinkle, R.T., Faulkner, J.A. and Chamberlain, J.S. (1995) Expression of full-length and truncated dystrophin mini-genes in transgenic mdx mice. *Hum. Mol. Genet.*, **4**, 1251–1258.
20. van Putten, M., Hulsker, M., Nadarajah, V.D., van Heiningen, S.H., van Huizen, E., van Iterson, M., Admiraal, P., Messemaker, T., den Dunnen, J.T., 't Hoen, P.A.C. *et al.* (2012) The effects of low levels of dystrophin on mouse muscle function and pathology. *PLoS One*, **7**, e31937.
21. Bonuccelli, G., Sotgia, F., Schubert, W., Park, D.S., Frank, P.G., Woodman, S.E., Insabato, L., Cammer, M., Minetti, C. and Lisanti, M.P. (2003) Proteasome inhibitor (MG-132) treatment of mdx mice rescues the expression and membrane localization of dystrophin and dystrophin-associated proteins. *Am. J. Pathol.*, **163**, 1663–1675.
22. Bonuccelli, G., Sotgia, F., Capozza, F., Gazzerro, E., Minetti, C. and Lisanti, M.P. (2007) Localized treatment with a novel FDA-approved proteasome inhibitor blocks the degradation of dystrophin and dystrophin-associated proteins in mdx mice. *Cell Cycle*, **6**, 1242–1248.
23. Briguet, A., Erb, M., Courdier-Fruh, I., Barzaghi, P., Santos, G., Herzner, H., Lescop, C., Siendt, H., Henneboehle, M., Weyermann, P. *et al.* (2008) Effect of calpain and proteasome inhibition on Ca^{2+}-dependent proteolysis and muscle histopathology in the mdx mouse. *FASEB J.*, **22**, 4190–4200.
24. Gazzerro, E., Assereto, S., Bonetto, A., Sotgia, F., Scarfì, S., Pistorio, A., Bonuccelli, G., Cilli, M., Bruno, C., Zara, F. *et al.* (2010) Therapeutic potential of proteasome inhibition in Duchenne and Becker muscular dystrophies. *Am. J. Pathol.*, **176**, 1863–1877.
25. Yang, J., Wang, Z., Fang, Y., Jiang, J., Zhao, F., Wong, H., Bennett, M.K., Molineaux, C.J. and Kirk, C.J. (2011) Pharmacokinetics, pharmacodynamics, metabolism, distribution, and excretion of carfilzomib in rats. *Drug Metab. Dispos.*, **39**, 1873–1882.
26. Stessman, H.A.F., Baughn, L.B., Sarver, A., Xia, T., Deshpande, R., Mansoor, A., Walsh, S.A., Sunderland, J.J., Dolloff, N.G., Linden, M.A. *et al.* (2013) Profiling bortezomib resistance identifies secondary therapies in a mouse myeloma model. *Mol. Cancer Ther.*, **12**, 1140–1150.
27. Hurchla, M.A., Garcia-Gomez, A., Hornick, M.C., Ocio, E.M., Li, A., Blanco, J.F., Collins, L., Kirk, C.J., Piwnica-Worms, D., Vij, R. *et al.* (2013) The epoxyketone-based proteasome inhibitors carfilzomib and orally bioavailable oprozomib have anti-resorptive and bone-anabolic activity in addition to anti-myeloma effects. *Leukemia*, **27**, 430–440.
28. Goldberg, A.L. (2007) Functions of the proteasome: from protein degradation and immune surveillance to cancer therapy. *Biochem. Soc. Trans.*, **35**, 12–17.
29. Goldberg, A.L. (2012) Development of proteasome inhibitors as research tools and cancer drugs. *J. Cell Biol.*, **199**, 583–588.
30. Weathington, N.M. and Mallampalli, R.K. (2014) Emerging therapies targeting the ubiquitin proteasome system in cancer. *J. Clin. Invest.*, **124**, 6–12.
31. Wells, D.J., Wells, K.E., Asante, E.A., Turner, G., Sunada, Y., Campbell, K.P., Walsh, F.S. and Dickson, G. (1995) Expression of human full-length and minidystrophin in transgenic mdx mice: implications for gene therapy of Duchenne muscular dystrophy. *Hum. Mol. Genet.*, **4**, 1245–1250.
32. Phelps, S.F., Hauser, M.A., Cole, N.M., Rafael, J.A., Hinkle, R.T., Faulkner, J.A. and Chamberlain, J.S. (1995) Expression of full-length and truncated dystrophin mini-genes in transgenic mdx mice. *Hum. Mol. Genet.*, **4**, 1251–1258.
33. Hollinger, K., Yang, C.X., Montz, R.E., Nonneman, D., Ross, J.W. and Selsby, J.T. (2014) Dystrophin insufficiency causes selective muscle histopathology and loss of dystrophin-glycoprotein complex assembly in pig skeletal muscle. *FASEB J.*, **28**, 1600–1609.
34. Li, D., Yue, Y. and Duan, D. (2008) Preservation of muscle force in Mdx3cv mice correlates with low-level expression of a near full-length dystrophin protein. *Am. J. Pathol.*, **172**, 1332–1341.
35. Kisselev, A.F., Callard, A. and Goldberg, A.L. (2006) Importance of the different proteolytic sites of the proteasome and the efficacy of inhibitors varies with the protein substrate. *J. Biol. Chem.*, **281**, 8582–8590.
36. Huang, J., Teng, L., Li, L., Liu, T., Li, L., Chen, D., Xu, L.-G., Zhai, Z. and Shu, H.-B. (2004) ZNF216 is an A20-like and IkappaB kinase gamma-interacting inhibitor of NFkappaB activation. *J. Biol. Chem.*, **279**, 16847–16853.
37. Hishiya, A., Iemura, S., Natsume, T., Takayama, S., Ikeda, K. and Watanabe, K. (2006) A novel ubiquitin-binding protein ZNF216 functioning in muscle atrophy. *EMBO J.*, **25**, 554–564.
38. Lutz, M., Wempe, F., Bahr, I., Zopf, D. and von Melchner, H. (2006) Proteasomal degradation of the multifunctional regulator YB-1 is mediated by an F-Box protein induced during programmed cell death. *FEBS Lett.*, **580**, 3921–3930.
39. Flood, W.D., Moyer, R.W., Tsykin, A., Sutherland, G.R. and Koblar, S.A. (2004) Nxf and Fbxo33: novel seizure-responsive genes in mice. *Eur. J. Neurosci.*, **20**, 1819–1826.
40. Geng, L.N., Yao, Z., Snider, L., Fong, A.P., Cech, J.N., Young, J.M., van der Maarel, S. M., Ruzzo, W.L., Gentleman, R.C., Tawil, R. *et al.* (2012) DUX4 activates germline genes, retroelements, and immune mediators: implications for facioscapulohumeral dystrophy. *Dev. Cell*, **22**, 38–51.
41. Wang, Y., Shirogane, T., Liu, D., Harper, J.W. and Elledge, S.J. (2003) Exit from exit: resetting the cell cycle through Amn1 inhibition of G protein signaling. *Cell*, **112**, 697–709.
42. Jin, Z., Li, R., Zhou, C., Shi, L., Zhang, X., Yang, Z., Zhang, D. and Sun, Q.-Y. (2016) Efficient gene knockdown in mouse oocytes through peptide nanoparticle-mediated SiRNA transfection. *PLoS One*, **11**, e0150462.
43. Bodine, S.C., Latres, E., Baumhueter, S., Lai, V.K., Nunez, L., Clarke, B.A., Poueymirou, W.T., Panaro, F.J., Na, E. and Dharmarajan, K. (2001) Identification of ubiquitin ligases required for skeletal muscle atrophy. *Science*, **294**, 1704–1708.
44. Lazzari, E. and Meroni, G. (2016) TRIM32 ubiquitin E3 ligase, one enzyme for several pathologies: From muscular dystrophy to tumours. *Int. J. Biochem. Cell Biol.*, **79**, 469–477.
45. Kwak, Y.-D., Wang, B., Li, J.J., Wang, R., Deng, Q., Diao, S., Chen, Y., Xu, R., Masliah, E., Xu, H. *et al.* (2012) Upregulation of the E3 ligase NEDD4-1 by oxidative stress degrades IGF-1 receptor protein in neurodegeneration. *J. Neurosci.*, **32**, 10971–10981.
46. Henderson, D.M., Belanto, J.J., Li, B., Heun-Johnson, H. and Ervasti, J.M. (2011) Internal deletion compromises the stability of dystrophin. *Hum. Mol. Genet.*, **20**, 2955–2963.
47. McCourt, J.L., Rhett, K.K., Jaeger, M.A., Belanto, J.J., Talsness, D.M. and Ervasti, J.M. (2015) *In vitro* stability of therapeutically relevant, internally truncated dystrophins. *Skelet. Muscle*, **5**, 13.
48. Liu, W. and Ralston, E. (2014) A new directionality tool for assessing microtubule pattern alterations. *Cytoskeleton*, **71**, 230–240.
49. Carlson, C.G. and Makiejus, R.V. (1990) A noninvasive procedure to detect muscle weakness in the mdx mouse. *Muscle Nerve*, **13**, 480–484.